Energy-pooling collisions in potassium: $4P_J+4P_J \rightarrow 4S+(nl=5P,6S,4D)$

R. K. Namiotka and J. Huennekens
Department of Physics, Lehigh University, 16 Memorial Drive East, Bethlehem, Pennsylvania 18015

M. Allegrini
Instituto Nazionale per la Fisica della Materia, Dipartimento di Fisica, Università di Pisa, Piazza Torricelli 2, 56126 Pisa, Italy and Dipartimento di Fisica della Materia e Tecnologie Fisiche Avanzate, Università di Messina, Salita Sperone 31, 98166 Sant' Agata, Messina, Italy

(Received 24 January 1997)

We report experimental rate coefficients for the energy-pooling collisions $K(4P_J)+K(4P_J)\rightarrow K(4S)+K(nl)$ with product states $nl=5P$, $6S$, and $4D$. The experimental procedure and analysis are similar to those used in a recent study of energy-pooling collisions in cesium. In potassium, it was found that $4P_{1/2}+4P_{1/2}$ collisions are more efficient than $4P_{3/2}+4P_{3/2}$ collisions for populating $5P$, while the opposite is true for populating $6S$. Since fluorescence from $4D$ was not seen, we can only report an upper limit for that rate coefficient. [S1050-2947(97)08307-8]

PACS number(s): 34.50.Rk, 34.90.+q

I. INTRODUCTION

When atomic vapors are resonantly excited by laser radiation, it is often possible to observe fluorescence from levels lying near twice the excitation energy [1]. Such fluorescence can result from ''energy-pooling'' (EP) collisions in which two excited atoms collide and ''pool'' their energy so that one atom ends in the ground state and the other in a more highly excited state. Since energy deficits or surpluses must be taken up by the kinetic energy of the colliding atoms, it is clear that the strongest EP collision processes will be those where the final energy state lies near twice the excitation energy. EP collisions have been studied extensively in alkali homonuclear [2–5] and heteronuclear [6,7] systems, as well as in other metal vapors [8–15] over the last 20 years. Measurements of EP cross sections at thermal energies provide important tests of theoretical molecular potential curves at large internuclear distances. The latter are of current interest in the study of ultracold atom collisions which occur at large separations.

Recently, we reported experimental rate coefficients for the EP process $Cs(6P_J)+Cs(6P_J)\rightarrow Cs(6S_{1/2})+Cs(nl_{J'})$ with product states $nl_{J'}=7P_{1/2}$, $7P_{3/2}$, $6D_{3/2}$, $6D_{5/2}$, $8S_{1/2}$, $4F_{5/2}$, and $4F_{7/2}$ [16]. The large fine-structure splitting of the cesium $6P_J$ energy levels allows the investigation of angular momentum propensity rules, since $Cs(6P_{1/2})+Cs(6P_{1/2})$, $Cs(6P_{1/2})+Cs(6P_{3/2})$, and $Cs(6P_{3/2})+Cs(6P_{3/2})$ can all be studied separately. Specifically, we found that $1/2+1/2$ collisions were more likely than $3/2+3/2$ collisions to populate the $7P$ levels, while $3/2+3/2$ collisions were more likely than $1/2+1/2$ collisions to populate $8S$. However, these results are consistent with the relative energy deficits (i.e., the energy deficit for populating $7P$ is much smaller for $1/2+1/2$ collisions than for $3/2+3/2$ collisions and vice versa for $8S$). Therefore it is not clear whether the relative size of the EP rate coefficients is primarily determined by energy deficits or whether angular momentum is also playing a role.

Here we report the results of an experimental investigation of potassium $K(4P_J)+K(4P_J)\rightarrow K(4S)+K(nl)$ EP collisions with product states $nl=5P$, $6S$, and $4D$. To the best of our knowledge, the only previous study of potassium EP collisions was presented in Ref. [17]. However, in that study, fluorescence from highly excited states could only be observed at high atom densities where significant ionization was also seen. Energy pooling could not be separated from associative ionization followed by dissociative recombination, as well as electron impact excitation, electron impact ionization, and electron-ion recombination. A model was developed [18] to take these various phenomena into account simultaneously, but only upper limits to the potassium EP cross sections could be obtained. On the other hand, potassium is of particular interest at the current time because new high-quality K_2 potentials have just become available [19], and these have recently been used to calculate cross sections for potassium EP collisions at temperatures around 1000 °C [20]. The calculations are now also being extended to lower temperatures appropriate to cell experiments [21]. Potassium is also interesting because the $4P_J$ fine-structure splitting is large enough to allow a separate study of the $4P_{1/2}+4P_{1/2}$ and $4P_{3/2}+4P_{3/2}$ collision processes (similar to the cesium case), but small compared to the EP collision energy deficits (unlike the cesium case). Thus the role of angular momentum in the EP process can be studied independently of energy deficits (see Fig. 1). Note that the $4P_J+4P_J$ energies lie almost half way between the exothermic $5P+4S$ product state and the endothermic $6S+4S$ and $4D+4S$ product states.

II. THEORY

The EP process can be modeled using rate equations, which are solved to yield steady-state level populations and the related fluorescence ratios. A complete model for cesium EP collisions has been presented in Ref. [16] where an expression for the EP rate coefficient in terms of the measured fluorescence ratios is given. Potassium $K(4P_J)+K(4P_J)\rightarrow K(4S)+K(nl)$ EP collisions can be treated

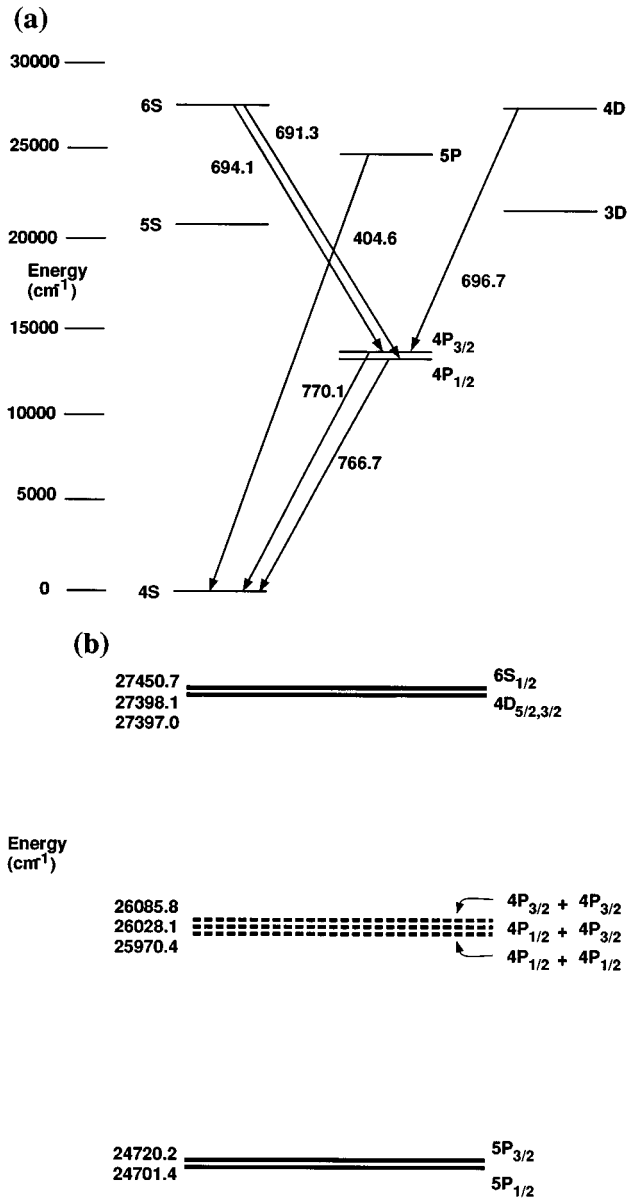

FIG. 1. (a) Potassium energy-level diagram. Arrows represent fluorescence transitions studied in this work. Wavelengths are given in nm. (b) Potassium atomic levels lying near twice the $4P_J$ level energies. $4P_J+4P_J$ energies are represented by dashed lines. Energies are taken from Ref. [29].

analogously to cesium $\mathrm{Cs}(6P_J)+\mathrm{Cs}(6P_J)\rightarrow\mathrm{Cs}(6S_{1/2})+\mathrm{Cs}(nl_{J'})$ collisions, and so here we only quote the result:

$$k_{nl}=\left(\frac{I_{nl\rightarrow n'l'_{J''}}/\varepsilon_{nl\rightarrow n'l'_{J''}}}{I_{4P_J\rightarrow 4S_{1/2}}/\varepsilon_{4P_J\rightarrow 4S_{1/2}}}\right)\times\frac{\lambda_{nl\rightarrow n'l'_{J''}}}{\lambda_{4P_J\rightarrow 4S_{1/2}}}\frac{\Gamma^{\mathrm{nat}}_{4P_J\rightarrow 4S_{1/2}}}{\Gamma^{\mathrm{nat}}_{nl\rightarrow n'l'_{J''}}}\frac{T_{4P_J\rightarrow 4S_{1/2}}}{T_{nl\rightarrow n'l'_{J''}}}\times\frac{2}{(\tau^{\mathrm{eff}}_{nl}/\tau^{\mathrm{nat}}_{nl})}\frac{\int_{-R}^{R}n_{4P_J}(x)dx}{\int_{-R}^{R}[n_{4P_J}(x)]^2dx}. \quad (1)$$

In this expression, $I_{nl\rightarrow n'l'_{J''}}$ is the fluorescence intensity corresponding to the transition $nl\rightarrow n'l'_{J''}$ emitted by atoms in the particular volume which is imaged onto the slits of our monochromator, $\varepsilon_{nl\rightarrow n'l'_{J''}}$ is the detection system efficiency (including effects due to the photomultiplier, monochromator grating, and any filters used) at the frequency of interest, $\Gamma^{\mathrm{nat}}_{nl\rightarrow n'l'_{J''}}$ is the natural radiative rate of the transition, and $\lambda_{nl\rightarrow n'l'_{J''}}$ is the transition wavelength. $T_{nl\rightarrow n'l'_{J''}}$ is the average probability that a photon emitted in the detection direction will pass through the vapor between its point of origin and the cell walls without being absorbed. It is related to the frequency-dependent absorption cross section (including hyperfine structure) and the density and spatial distribution of atoms in the lower level of the transition, and is given explicitly in Eqs. (8)–(11) of Ref. [16]. We note that in the present potassium experiment, $T_{nl\rightarrow n'l'_{J''}}$ is approximately equal to 1 except for the $4P_J\rightarrow 4S_{1/2}$ resonance transitions. τ^{nat}_{nl} is the natural lifetime of level nl, and τ^{eff}_{nl} is the effective lifetime of level nl including the effects of radiation trapping. The latter is calculated using the Molisch theory of radiation trapping [22,23], and these calculations are also described in detail in Ref. [16]. However, in the present case, trapping on all transitions of interest is negligible [i.e., $(\tau^{\mathrm{eff}}_{nl}/\tau^{\mathrm{nat}}_{nl})\sim 1$ for all transitions of interest—see Table I]. Finally, $n_{4P_J}(x)$ is the position-dependent excited atom density and R is the radius of the cylindrical cell. Note that the fluorescence volume integrals in Eq. (1) have been reduced to one-dimensional integrals since the excitation is independent of position along the cell axis and fluorescence is detected from a thin strip across the cell (see next section and Fig. 2). Experimentally, the measured quantities are $I_{nl\rightarrow n'l'_{J''}}$, $\varepsilon_{nl\rightarrow n'l'_{J''}}$, $I_{4P_J\rightarrow 4S_{1/2}}$, $\varepsilon_{4P_J\rightarrow 4S_{1/2}}$, and $n_{4P_J}(x)$.

III. EXPERIMENT

The experimental setup for the potassium EP rate coefficient measurements is shown in Fig. 2, and is almost identical to that used for the cesium measurements described in Ref. [16]. In the interest of brevity, the reader is referred to Ref. [16] for details. Potassium vapor was contained in a cylindrical glass cell, 81 mm long and 20 mm in diameter, with no buffer gas. The cell was heated to 94–120 °C, producing a potassium density of $0.3–1.8\times10^{12}$ cm^{-3} in the vapor phase according to the Nesmeyanov relation [24]. Accurate determination of the ground-state density using optical absorption measurements is difficult in this temperature range where the resonance lines are optically thick. However, measurements of the $4S_{1/2}\rightarrow 4P_{3/2}$ transition line center absorption coefficient in the temperature range 46–55 °C indicated that the actual potassium atom number density was approximately 22% higher than the values given by the Nesmeyanov formula. In the analysis which follows, we assume that the atom density in the experimental temperature range 94–120 °C was also 22% greater than values obtained from Nesmeyanov, with ~25% uncertainty.

A single-mode, cw Ti:sapphire laser (Coherent model 899-29) was used to pump either the D_1 ($4S_{1/2}\rightarrow 4P_{1/2}$) or D_2 ($4S_{1/2}\rightarrow 4P_{3/2}$) potassium resonance transition. Typical

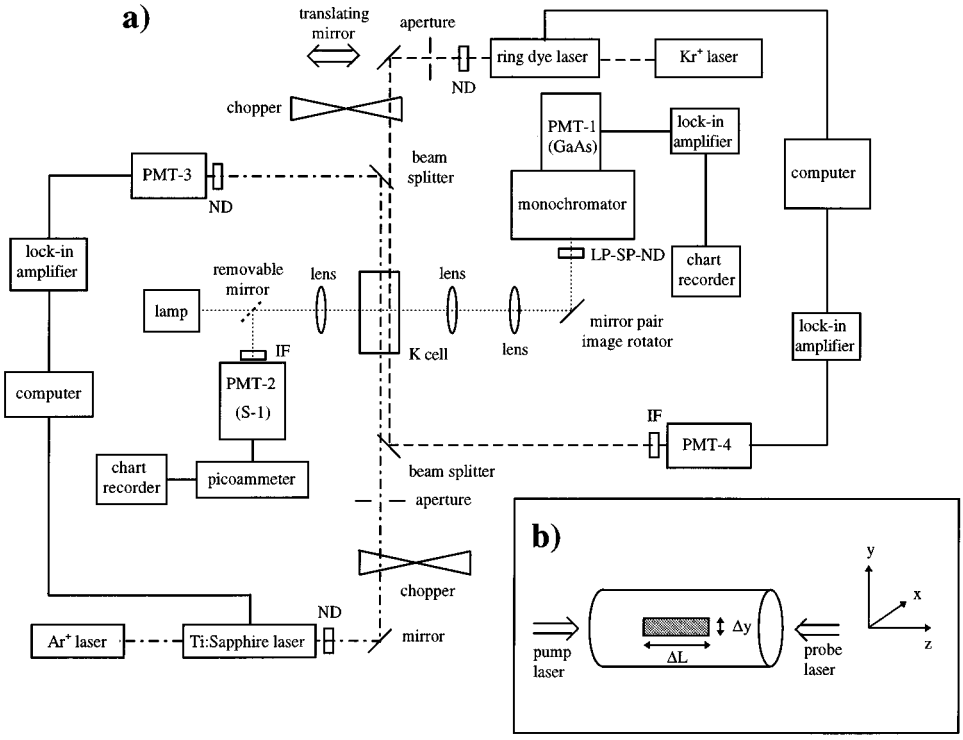

FIG. 2. (a) Experimental setup. The Ti:sapphire laser was used to pump the potassium $4S_{1/2}\rightarrow 4P_J$ resonance transition. The monochromator and photomultiplier tube (PMT-1) were used to spectrally resolve the potassium atomic line fluorescence. PMT-2 was used to monitor total resonance line (D_1 or D_2) fluorescence, and PMT-3 monitored the transmission of the Ti:sapphire beam through the cell. The ring dye laser was used to probe the $4P_J$ level density at various positions in the cell (determined by the position of the translating mirror). PMT-4 was used to monitor the dye laser transmission. IF, LP, SP, and ND represent interference, long-pass, short-pass, and neutral-density filter, respectively. (b) Inset showing the cell geometry and the region (shaded) from which fluorescence was detected. The height of the imaged region is $\Delta y\sim 150\ \mu$m and the length $\Delta L\sim 0.5$ cm.

laser powers were 700 mW for the D_1 line and 600 mW for the D_2 line in a roughly collimated 8-mm-diam beam. The frequency of the pump laser was set to maximize the $4P_J\rightarrow 4S_{1/2}$ fluorescence from the observation region. The attenuation over the observation region was negligible. Thus the excited atom density could be considered constant along the beam axis.

The setup for detection of fluorescence was the same as described in Ref. [16]. Resolved $4P_J\rightarrow 4S_{1/2}$, $5P\rightarrow 4S_{1/2}$, $6S_{1/2}\rightarrow 4P_{1/2}$, $6S_{1/2}\rightarrow 4P_{3/2}$, and $4D_{5/2}\rightarrow 4P_{3/2}$ fluorescence, emitted in the region of the cell volume indicated in Fig. 2(b), was recorded at each temperature for both D_1 and D_2 pumping, using a monochromator (Spex model 1681, 0.22 m) with attached photomultiplier tube (Hamamatsu model R636 GaAs, PMT-1 in Fig. 2). Monochromator slits were set to 300–500 μm (1–2 nm resolution). Thus the $5P_{J'}\rightarrow 4S_{1/2}$ fine-structure transitions could not be resolved. A short-pass filter (Reynard) with cut-on wavelength of 700 nm or a 680–740 nm bandpass filter (Melles Griot) was used to block scattered D_1 and D_2 line fluorescence when recording the EP fluorescence signals. Calibrated neutral density filters were used to attenuate the strong D_1 and D_2 signals so that they could be recorded using the same monochromator slits and photomultiplier tube (PMT) voltage. The wavelength-dependent relative detection-system efficiency ε, including the effects of all filters, was measured using a calibrated tungsten-halogen lamp [25]. A free-standing photomultiplier tube (Hamamatsu R406, PMT-2 in Fig. 2) was used to monitor the total D_1 and D_2 fluorescence throughout the experiment in order to guard against frequency or intensity drift of the pump laser.

A single-mode cw dye laser (Coherent 699-29, using LD-700 dye pumped by a 6-W krypton ion laser) was used to probe the density and spatial distribution of the atoms in the $4P_J$ levels. The power of the probe laser was cut down to $\sim$20 nW with neutral density filters. We directly measure the $4P_{3/2}$ number density by scanning the probe laser over the $4P_{3/2}\rightarrow 6S_{1/2}$ transition and monitoring its transmission using another photomultiplier tube (PMT-4). In order to measure the spatial dependence $n_{4P_{3/2}}(x)$ across the diameter of the cell, the probe laser was stepped across the cell parallel to the pump beam using the translating mirror shown in the figure.

The transmitted intensity of the probe-laser beam through a length L of the vapor is given by

$$I_\nu(L)=I_\nu(0)e^{-k_{6S_{1/2}\leftarrow 4P_{3/2}}(\nu)L} \tag{2}$$

for light of frequency ν. Here $I_\nu(0)$ is the incident intensity and $k_{6S_{1/2}\leftarrow 4P_{3/2}}(\nu)$ is the frequency-dependent absorption coefficient. $n_{4P_{3/2}}$ is related to the integral of

TABLE I. Measured rate coefficients for the potassium energy-pooling collisions $K(4P_J)+K(4P_J)\rightarrow K(4S_{1/2})+K(nl)$.

$K(4P_{3/2})+K(4P_{3/2})\rightarrow K(4S_{1/2})+K(nl)$

nl	Temperature (°C)	$n_{4S_{1/2}}$ (10^{11} cm^{-3})	$T_{4P_{3/2}\rightarrow 4S_{1/2}}$	$\frac{\int_{-R}^{R} n_{4P_{3/2}}(x)dx}{\int_{-R}^{R}[n_{4P_{3/2}}(x)]^2dx}$	Monitored transition $nl\rightarrow n'l'_{J''}$	$\frac{I_{nl\rightarrow n'l'_{J''}}/\varepsilon_{nl\rightarrow n'l'_{J''}}}{I_{4P_{3/2}\rightarrow 4S_{1/2}}/\varepsilon_{4P_{3/2}\rightarrow 4S_{1/2}}}$	$T_{nl\rightarrow n'l'_{J''}}$	$\frac{\tau_{nl}^{\text{eff}}}{\tau_{nl}^{\text{nat}}}$	k_{nl} (cm^3 s^{-1})
$5P$	94	3.61	0.0945	$(3.49\times10^{10})^{-1}$	$5P\rightarrow 4S_{1/2}$	3.71×10^{-8}	0.973	1.004	2.49×10^{-11}
	105	8.03	0.0449	$(5.72\times10^{10})^{-1}$		2.21×10^{-7}	0.943	1.009	4.41×10^{-11}
	118	19.46	0.0133	$(1.41\times10^{11})^{-1}$		1.97×10^{-6}	0.866	1.021	5.08×10^{-11}
$6S$	105	8.03	0.0449	$(5.72\times10^{10})^{-1}$	$6S\rightarrow 4P_{1/2}$	4.21×10^{-8}	1.000	1.004	1.09×10^{-11}
	118	19.46	0.0133	$(1.41\times10^{11})^{-1}$		2.88×10^{-7}	1.000	1.009	8.92×10^{-12}
	120	22.18				8.88×10^{-8}	1.000	1.009	3.87×10^{-12} [a]
	105	8.03	0.0449	$(5.72\times10^{10})^{-1}$	$6S\rightarrow 4P_{3/2}$	9.46×10^{-8}	0.990	1.004	1.25×10^{-11}
	118	19.46	0.0133	$(1.41\times10^{11})^{-1}$		5.37×10^{-7}	0.979	1.009	8.59×10^{-12}
	120	22.18				1.85×10^{-7}	0.979	1.009	4.17×10^{-12} [a]
$4D$	120	22.18			$4D_{5/2}\rightarrow 4P_{3/2}$	$<2\times10^{-8}$	1.000	1.000	$<2.0\times10^{-11}$ [a]

$K(4P_{1/2})+K(4P_{1/2})\rightarrow K(4S_{1/2})+K(nl)$

nl	Temperature (°C)	$n_{4S_{1/2}}$ (10^{11} cm^{-3})	$T_{4P_{1/2}\rightarrow 4S_{1/2}}$	$\frac{\int_{-R}^{R} n_{4P_{1/2}}(x)dx}{\int_{-R}^{R}[n_{4P_{1/2}}(x)]^2dx}$	Monitored transition $nl\rightarrow n'l'_{J''}$	$\frac{I_{nl\rightarrow n'l'_{J''}}/\varepsilon_{nl\rightarrow n'l'_{J''}}}{I_{4P_{1/2}\rightarrow 4S_{1/2}}/\varepsilon_{4P_{1/2}\rightarrow 4S_{1/2}}}$	$T_{nl\rightarrow n'l'_{J''}}$	$\frac{\tau_{nl}^{\text{eff}}}{\tau_{nl}^{\text{nat}}}$	k_{nl} (cm^3 s^{-1})
$5P$	95	3.89	0.1724	$(3.33\times10^{10})^{-1}$	$5P\rightarrow 4S_{1/2}$	1.08×10^{-7}	0.970	1.005	1.37×10^{-10}
	105	8.03	0.0635	$(1.07\times10^{11})^{-1}$		7.00×10^{-7}	0.940	1.009	1.04×10^{-10}
	118	19.46	0.0236	$(2.02\times10^{11})^{-1}$		1.59×10^{-6}	0.863	1.021	5.01×10^{-11}
$6S$	105	8.03	0.0635	$(1.07\times10^{11})^{-1}$	$6S\rightarrow 4P_{1/2}$	2.78×10^{-8}	0.988	1.002	5.44×10^{-12}
	118	19.46	0.0236	$(2.02\times10^{11})^{-1}$		4.28×10^{-8}	0.976	1.004	1.66×10^{-12}
	120	22.18				4.10×10^{-8}	0.976	1.004	1.10×10^{-12} [a]
	105	8.03	0.0635	$(1.07\times10^{11})^{-1}$	$6S\rightarrow 4P_{3/2}$	5.37×10^{-8}	1.000	1.002	5.26×10^{-12}
	118	19.46	0.0236	$(2.02\times10^{11})^{-1}$		8.89×10^{-8}	1.000	1.004	1.71×10^{-12}
	120	22.18				6.28×10^{-8}	1.000	1.004	8.36×10^{-13} [a]
$4D$	120	22.18			$4D_{5/2}\rightarrow 4P_{3/2}$	$<2\times10^{-8}$	1.000	1.000	$<1.2\times10^{-11}$ [a]

[a]Results obtained relative to k_{5P} from the relation

$$k_{nl}=k_{5P}\left(\frac{I_{nl\rightarrow n'l'_{J''}}/\varepsilon_{nl\rightarrow n'l'_{J''}}}{I_{5P\rightarrow 4S_{1/2}}/\varepsilon_{5P\rightarrow 4S_{1/2}}}\right)\frac{\lambda_{nl\rightarrow n'l'_{J''}}}{\lambda_{5P\rightarrow 4S_{1/2}}}\frac{\Gamma^{\text{nat}}_{5P\rightarrow 4S_{1/2}}\tau^{\text{nat}}_{5P}}{\Gamma^{\text{nat}}_{nl\rightarrow n'l'_{J''}}\tau^{\text{nat}}_{nl}}\frac{T_{5P\rightarrow 4S_{1/2}}(\tau^{\text{eff}}_{5P}/\tau^{\text{nat}}_{5P})}{T_{nl\rightarrow n'l'_{J''}}(\tau^{\text{eff}}_{nl}/\tau^{\text{nat}}_{nl})}$$

with $(I_{5P\rightarrow 4S_{1/2}}/\varepsilon_{5P\rightarrow 4S_{1/2}})/(I_{4P_J\rightarrow 4S_{1/2}}/\varepsilon_{4P_J\rightarrow 4S_{1/2}})=1.4\times10^{-6}$ for D_2 pumping and $(I_{5P\rightarrow 4S_{1/2}}/\varepsilon_{5P\rightarrow 4S_{1/2}})/(I_{4P_J\rightarrow 4S_{1/2}}/\varepsilon_{4P_J\rightarrow 4S_{1/2}})=2.3\times10^{-6}$ for D_1 pumping.

$k_{6S_{1/2}\leftarrow 4P_{3/2}}(\nu)$ by [26]

$$\int k_{6S_{1/2}\leftarrow 4P_{3/2}}(\nu)d\nu = \frac{[\lambda_{6S_{1/2}\rightarrow 4P_{3/2}}]^2}{8\pi}\frac{g_{6S_{1/2}}}{g_{4P_{3/2}}}n_{4P_{3/2}}\Gamma^{\text{nat}}_{6S_{1/2}\rightarrow 4P_{3/2}}, \quad (3)$$

where $g_{6S_{1/2}}$ and $g_{4P_{3/2}}$ are the degeneracies of the $6S_{1/2}$ and $4P_{3/2}$ states, respectively. Thus we can extract $n_{4P_{3/2}}(x)$ from the position dependent probe transmission scans using Eqs. (2) and (3).

Due to weak oscillator strengths of probe transitions within the wavelength range of the dye laser, we were unable to measure absorption from the $4P_{1/2}$ state directly. Instead, we monitored cascade $5P\rightarrow 4S$ fluorescence as the probe laser was scanned across the $4P_{1/2}\rightarrow 4D_{3/2}$ transition. This allowed a relative measurement of the excited atom spatial distribution, $n_{4P_{1/2}}(x)$. The measurement was placed on an absolute scale by comparing the ratio of D_2 fluorescence under conditions where the absolute $4P_{3/2}$ density and spatial distribution were known (D_2 pumping, no probe laser) to D_1 fluorescence where only the relative $4P_{1/2}$ spatial distribution was known (D_1 pumping, no probe laser). Specifically,

TABLE II. Values for the potassium energy-pooling rate coefficients and cross sections obtained in this work. The error bars reflect statistical uncertainties only. Including systematic effects we estimate that the EP rate coefficients are only accurate to ~50%, with the exception of the $6S$ rate coefficient for D_1 pumping (where the uncertainties are −80%).

$K(4P_{3/2})+K(4P_{3/2})\rightarrow K(4S_{1/2})+K(nl)$		
nl	Rate coefficients ($cm^3\,s^{-1}$)	Cross sections (cm^2)
$5P$	$(4.0\pm1.3)\times10^{-11}$	$(6.2\pm2.1)\times10^{-16}$
$6S$	$(8.2\pm3.5)\times10^{-12}$	$(1.3\pm0.5)\times10^{-16}$
$4D$	$<2.0\times10^{-11}$	$<3.1\times10^{-16}$

$K(4P_{1/2})+K(4P_{1/2})\rightarrow K(4S_{1/2})+K(nl)$		
nl	Rate coefficients ($cm^3\,s^{-1}$)	Cross sections (cm^2)
$5P$	$(9.7\pm4.4)\times10^{-11}$	$(1.5\pm0.7)\times10^{-15}$
$6S$	$(2.7\pm2.1)\times10^{-12}$	$(4.2\pm3.3)\times10^{-17}$
$4D$	$<1.2\times10^{-11}$	$<1.8\times10^{-16}$

$$\frac{(I_{4P_{1/2}\rightarrow4S_{1/2}}/\varepsilon_{4P_{1/2}\rightarrow4S_{1/2}})_{D_1\text{ pump}}}{(I_{4P_{3/2}\rightarrow4S_{1/2}}/\varepsilon_{4P_{3/2}\rightarrow4S_{1/2}})_{D_2\text{ pump}}} = \frac{\lambda_{4P_{3/2}\rightarrow4S_{1/2}}}{\lambda_{4P_{1/2}\rightarrow4S_{1/2}}} \times\frac{[T_{4P_{1/2}\rightarrow4S_{1/2}}]_{D_1\text{ pump}}\Gamma^{\text{nat}}_{4P_{1/2}\rightarrow4S_{1/2}}}{[T_{4P_{3/2}\rightarrow4S_{1/2}}]_{D_2\text{ pump}}\Gamma^{\text{nat}}_{4P_{3/2}\rightarrow4S_{1/2}}} \times\frac{[n_{4P_{1/2}}(x=0)]_{D_1\text{ pump}}\int_{-R}^{R}[n^{\text{rel}}_{4P_{1/2}}(x)]_{D_1\text{ pump}}dx}{\int_{-R}^{R}[n_{4P_{3/2}}(x)]_{D_2\text{ pump}}dx}. \tag{4}$$

Here $[n_{4P_{3/2}}(x)]_{D_2\text{ pump}}$ is the absolute $4P_{3/2}$ density distribution measured in the D_2 pump case, $[n^{\text{rel}}_{4P_{1/2}}(x)]_{D_1\text{ pump}}$ is the relative $4P_{1/2}$ spatial distribution (normalized to one on the cell axis, $x=0$) measured in the D_1 pump case, and $[n_{4P_{1/2}}(x=0)]_{D_1\text{ pump}}$ is the unknown absolute $4P_{1/2}$ density on the cell axis in the D_1 pump case. The transmission factors are calculated as described in Ref. [16]. Thus we can find $[n_{4P_{1/2}}(x=0)]_{D_1\text{ pump}}$ from our measurements of $[n^{\text{rel}}_{4P_{1/2}}(x)]_{D_1\text{ pump}}$, $[n_{4P_{3/2}}(x)]_{D_2\text{ pump}}$, and the D_1 to D_2 line fluorescence ratio.

IV. RESULTS AND DISCUSSION

The excited atom density spatial distributions were integrated numerically as required in Eq. (1) and then combined with the measured fluorescence ratios, calculated transmission factors, and calculated effective lifetimes to yield values for the EP rate coefficients. The various rate coefficients for each temperature are listed in Table I. Only an upper limit for k_{4D} was obtained since we were unable to detect $4D_{5/2}\rightarrow4P_{3/2}$ fluorescence with our highest sensitivity. The procedures used to calculate transmission factors and the relatively minor radiation trapping corrections to the high-lying state lifetimes were the same as those used in the analysis of the cesium experiment [16]. In the case of potassium, natural radiative rates for all transitions were taken from Wiese *et al.* [27]. Resonance–broadening rates (needed in the numerical calculations of $T_{4P_J\rightarrow4S_{1/2}}$) were taken from Carrington, Stacey, and Cooper [28].

The statistical errors in the potassium measurements are also similar to those of the cesium measurements. We estimate a 25% uncertainty in all fluorescence ratios with the exception of the $6S$ fluorescence ratio for D_1 pumping where we estimate a 50% uncertainty because the signals were extremely weak. We estimate the uncertainties in the ratio $\int_{-R}^{R}n_{4P_J}(x)dx/\int_{-R}^{R}[n_{4P_J}(x)]^2dx$ to be approximately 15% for $J=3/2$ and 25% for $J=1/2$ since the determination is less direct in the latter case. The ground-state hyperfine splitting in potassium is smaller than the Doppler linewidth. Thus hyperfine optical pumping is much less significant than in cesium and this allowed us to observe EP fluorescence with lower ground-state densities. As a result, the effects of radiation trapping were greatly reduced and we estimate uncertainties in the factor $T_{nl\rightarrow n'l'_{J''}}(\tau^{\text{eff}}_{nl}/\tau^{\text{nat}}_{nl})$ to be about 5%. Similarly, we estimate that values of $T_{4P_J\rightarrow4S_{1/2}}$ are good to about 30%. Possible systematic effects include the uncertainty in the ground-state density determination (which affects $T_{4P_J\rightarrow4S_{1/2}}$), neglect of cascade from higher levels, and mixing of product state populations due to collisions with ground-state potassium or impurity atoms. Using large $6S,4D\rightarrow5P$ and $4D\rightarrow6S$ mixing rate coefficients ($3\times10^{-10}\ cm^3\,sec^{-1}$) and impurity densities ($10^{15}\ cm^{-3}$) and assuming the $4D$ population is the maximum allowed by our upper limit of k_{4D}, we estimate that the $6S\rightarrow5P$ cascade and $6S,4D\rightarrow5P$ mixing terms contribute less than 10% to the uncertainty in our k_{5P} values. Based on these worst-case considerations, the $4D\rightarrow5P$ cascade may contribute up to 50% and 13% uncertainty to k_{5P}, and $4D\rightarrow6S$ mixing may contribute up to 20% and 34% uncertainty to k_{6S}, in the D_2 and D_1 pumping cases, respectively. These are upper limits, of course, since we observed no detectable $4D$ fluorescence.

The rate coefficients defined by Eq. (1) are based on the assumption that only one $4P_J$ fine-structure level is popu-

lated, i.e., the we only observe $4P_{3/2}+4P_{3/2}$ EP collisions for D_2 line pumping and $4P_{1/2}+4P_{1/2}$ EP collisions for D_1 line pumping. However, due to collisions with impurity atoms and ground-state potassium atoms, excitation transfer occurs between the $4P_J$ fine-structure levels. Thus, even though we pump only one fine-structure level at a time, some population also exists in the other fine-structure level. Consequently, our results may be contaminated by contributions from $4P_{3/2}+4P_{1/2}$ collisions. However, our measurements show that the population in the collisionally populated level never exceeds 20% of the population in the directly pumped level (except at the highest temperature in the D_1 pump case). Since $4P_{3/2}+4P_{1/2}$ is no more resonant than $4P_{1/2}+4P_{1/2}$ or $4P_{3/2}+4P_{3/2}$ collisions (unlike the situation in cesium), we do not believe that neglect of $4P_{3/2}+4P_{1/2}$ collisions introduces much uncertainty into our results.

Considering the various sources of uncertainty, including possible systematic errors, we estimate overall uncertainties of $\sim$50% in our measured energy-pooling rate coefficients, with the exception of the $6S$ rate coefficient for D_1 pumping (where the uncertainties are $\sim$80%).

V. CONCLUSIONS

Final EP rate coefficients obtained in this work (by averaging all data collected over the range 94–120 °C) are presented in Table II along with cross sections obtained from the relation $k_{nl}=\langle\sigma_{nl}v\rangle\approx\sigma_{nl}\langle v\rangle$. The results of Table II show some interesting similarities to those obtained in cesium. Specifically, the $5P$ state is populated more effectively by $4P_{1/2}+4P_{12}$ collisions than by $4P_{3/2}+4P_{3/2}$ collisions. In cesium we found that the analogous $7P$ state is more effectively populated by $6P_{1/2}+6P_{1/2}$ collisions than by $6P_{3/2}+6P_{3/2}$ collisions. Similarly, in potassium we find that $6S$ is populated more effectively by $4P_{3/2}+4P_{3/2}$ collisions, which is analogous to the cesium case, where $8S$ is populated more effectively by $6P_{3/2}+6P_{3/2}$ collisions. In the case of cesium it appeared that these results could be explained strictly on the basis of energy deficits: $6P_{3/2}+6P_{3/2}$ is more resonant than $6P_{1/2}+6P_{1/2}$ with $8S$, while $6P_{1/2}+6P_{1/2}$ is more resonant than $6P_{3/2}+6P_{3/2}$ with $7P$ [see Fig. 1(b) in Ref. [16]]. In potassium, the energy deficits are nearly the same [see Fig. 1(b) of the present manuscript], and thus the differences for $4P_{1/2}+4P_{1/2}$ vs $4P_{3/2}+4P_{3/2}$ collisions may indicate that angular momentum propensity rules can play a role in the EP process. Such propensity rules were not found in earlier studies of EP in strontium and barium [10,12,15]. Another interesting result of the cesium experiment is the fact that $7P_{1/2}$ is much more strongly populated than $7P_{3/2}$ in $6P_{1/2}+6P_{1/2}$ collisions, while the two $7P_{J'}$ levels are approximately equally populated by $6P_{3/2}+6P_{3/2}$ collisions. We had hoped to see if an analogous result occurred in potassium. However, the potassium $5P_{J'}$ EP signals were too small to measure at the densities and monochromator slit widths necessary to resolve the fine-structure levels. At higher densities, the $5P_{J'}\rightarrow 4S_{1/2}$ fluorescence is spectrally broadened by self-absorption in the vapor. Thus the $5P_{J'}$ levels cannot be separately resolved. Finally, in cesium we found that the $6D$ levels are populated more efficiently through EP than any other excited states, while in potassium we were unable to detect any fluorescence from the analogous $4D$ levels. This can most likely be attributed to the fact that in cesium $6P_J+6P_J\rightarrow 6S_{1/2}+6D_{J'}$ is almost resonant, while the potassium $4P_J+4P_J\rightarrow 4S_{1/2}+4D_{J'}$ energy deficit is much larger.

The only previous experimental determination of EP cross sections in potassium were the upper limits $\sigma_{6S}\leqslant 6\times10^{-16}$ cm^2 and $\sigma_{4D}\leqslant 8\times10^{-16}$ cm^2 obtained from the theoretical model [18] of the cw experiment presented in Ref. [17]. We note that these limits are consistent with the cross sections obtained in the present work. The cross sections have also been obtained theoretically in Ref. [20], but only for mean collision velocities greater than 1200 m/sec (corresponding to temperatures in excess of 1000 °C). The calculations show that the thermally averaged cross sections at these temperatures are $\sigma_{4D}\sim 6\times10^{-16}$ cm^2, $\sigma_{6S}\sim 2.4\times10^{-17}$ cm^2, and $\sigma_{5P}\sim 6\times10^{-17}$ cm^2. However, the EP processes which populate $4D$ and $6S$ are strongly endothermic, so that both cross sections should be much smaller at the temperatures of the present experiment ($\sim$100 °C). Conversely, the EP process which populates $5P$ is exothermic and the calculations show that the cross section rises as the mean velocity decreases. Thus it is difficult to compare the experimental and theoretical cross sections at the present time. However, theoretical calculations of the EP cross sections at lower temperatures are currently underway [21], and a meaningful comparison should be possible in the near future. Finally, we should note that the current theoretical calculations [20] do not include the $4P$ state fine structure. Because of the apparent angular momentum propensity rules seen in this work and in Ref. [16], it would be extremely interesting to extend the theoretical work to include fine-structure effects.

ACKNOWLEDGMENTS

The authors would like to thank Dr. Francoise Masnou-Seeuws and Dr. Sylvie Magnier for making their results available to us prior to publication. This work was supported by the National Science Foundation through Grant No. PHY9119498.

[1] M. Allegrini, G. Alzetta, A. Kopystynska, L. Moi, and G. Orriols, Opt. Commun. **19**, 96 (1976).

[2] For a review of alkali-atom energy-pooling cross section measurements until 1985, see M. Allegrini, C. Gabbanini, and L. Moi, J. Phys. (France) Colloq. **46**, C1-61 (1985).

[3] M. Allegrini, C. Gabbanini, L. Moi, and R. Colle, Phys. Rev. A **32**, 2068 (1985).

[4] S. A. Davidson, J. F. Kelly, and A. Gallagher, Phys. Rev. A **33**, 3756 (1986).

[5] C. He and R. A. Bernheim, Chem. Phys. Lett. **190**, 494 (1992).

[6] S. Gozzini, S. A. Abdullah, M. Allegrini, A. Cremoncini, and L. Moi, Opt. Commun. **63**, 97 (1987).
[7] C. Gabbanini, S. Gozzini, G. Squadrito, M. Allegrini, and L. Moi, Phys. Rev. A **39**, 6148 (1989).
[8] W. H. Breckenridge, W. L. Nikolai, and J. Stewart, J. Chem. Phys. **74**, 2073 (1981).
[9] H. Umemoto, J. Kikuma, A. Masaki, and S. Sato, Chem. Phys. **127**, 227 (1988).
[10] J. F. Kelly, M. Harris, and A. Gallagher, Phys. Rev. A **38**, 1225 (1988).
[11] S. Majetich, C. A. Tomczyk, and J. R. Wiesenfeld, Phys. Rev. A **41**, 6085 (1990).
[12] H. G. C. Werij, M. Harris, J. Cooper, A. Gallagher, and J. F. Kelly, Phys. Rev. A **43**, 2237 (1991).
[13] B. Cheng, Z. Li, Y. Yang, J. Zhu, and D. Zhang, Opt. Commun. **86**, 465 (1991).
[14] P. Bicchi, C. Marinelli, E. Mariotti, M. Meucci, and L. Moi, J. Phys. B **26**, 2335 (1993).
[15] J. A. Neuman, A. Gallagher, and J. Cooper, Phys. Rev. A **50**, 1292 (1994).
[16] Z. J. Jabbour, R. K. Namiotka, J. Huennekens, M. Allegrini, S. Milošević, and F. de Tomasi, Phys. Rev. A **54**, 1372 (1996).
[17] M. Allegrini, S. Gozzini, I. Longo, P. Savino, and P. Bicchi, Nuovo Cimento D **1**, 49 (1982).
[18] F. Giammanco and S. Gozzini, Nuovo Cimento B **66**, 47 (1981).
[19] S. Magnier and Ph. Millié, Phys. Rev. A **54**, 204 (1996).
[20] Yu. Yurova, S. Magnier, Ph. Millié, O. Dulieu, and F. Masnou-Seeuws (unpublished).
[21] S. Magnier and F. Masnou-Seeuws (private communication).
[22] A. F. Molisch, B. P. Oehry, and G. Magerl, J. Quant. Spectrosc. Radiat. Transf. **48**, 377 (1992).
[23] A. F. Molisch, B. P. Oehry, W. Schupita, and G. Magerl, J. Quant. Spectrosc. Radiat. Transf. **49**, 361 (1993).
[24] A. N. Nesmeyanov, *Vapour Pressure of the Elements* (Academic, New York, 1963).
[25] R. Stair, W. E. Schneider, and J. K. Jackson, Appl. Opt. **2**, 1151 (1963).
[26] A. C. G. Mitchell and M. W. Zemansky, *Resonance Radiation and Excited Atoms* (Cambridge University Press, New York, 1971), p. 116.
[27] W. L. Wiese, M. W. Smith, and B. M. Miles, *Atomic Transition Probabilities*, National Bureau of Standards, National Standard Reference Data Series, No. 22 (U.S. GPO, Washington, D.C., 1969), Vol. II.
[28] C. G. Carrington, D. N. Stacey, and J. Cooper, J. Phys. B **6**, 417 (1973).
[29] C. E. Moore, *Atomic Energy Levels*, Natl. Bur. Stand. (U.S.) Circ. No. 467 (U.S. GPO, Washington, D.C., 1948, 1952, and 1958), Vols. I–III.